

Vision-based Autonomous Tracking and Landing of a Fully-actuated Rotorcraft

Mahathi Bhargavapuri^a, Animesh Kumar Shastry^b, Harsh Sinha^b, Soumya Ranjan Sahoo^a, Mangal Kothari^{b,*}

^a*Dept. of Electrical Engineering, Indian Institute of Technology Kanpur, Kanpur, India.*

^b*Dept. of Aerospace Engineering, Indian Institute of Technology Kanpur, Kanpur, India.*

Abstract

Autonomous landing a challenging phase of flight for an aerial vehicle, especially when attempting to land on a moving target. This paper presents vision-based tracking and landing of a fully-actuated tilt-augmented quadrotor on a moving target. A fully-actuated vehicle allows higher freedom in terms of control design and larger flight envelope since the position and attitude states are decoupled. An adaptive control law is designed to track a moving target with only relative position information from a camera. Low-cost hardware is used and experiments are carried out to validate the proposed methodology for targets moving at realistic speeds.

Keywords: Autonomous Systems, Unmanned Aerial Vehicles, Vision, Autonomous Landing, Aerospace Control.

Video of the real-world experiments conducted (both indoor and outdoor) can be found at <https://youtu.be/Czgc6OZPnDw> .

1. Introduction

The use of rotary wing unmanned aerial vehicles (RUAVs) with the ability to vertically take-off and land (VTOL) has been widespread in the areas of rescue and reconnaissance, package delivery, inspection of bridges and other hazardous

*Corresponding author
Email address: mangal@iitk.ac.in (Mangal Kothari)

environments, and so on. For a majority of such applications, a RUAU working in cooperation with a ground vehicle would be highly advantageous. A few advantages of such a collaboration of vehicles are larger range of operations, increased flight time, and higher efficiency [1–3]. In this work, a RUAU can refer to a conventional helicopter type or a multi-rotor type UAV.

1.1. Background and Motivation

The tasks of take-off, target following, and landing of the RUAU in such teams of heterogeneous vehicles have to be performed autonomously in most cases. Of these, the tracking and landing phases of the flight are highly challenging and abundant research regarding the same has been carried out. Long range tracking can be done using GPS. However, for smaller range of operations, GPS becomes a liability during precision tracking and landing since it contributes to large covariance in measurements for localization. GPS is also unreliable in closed spaces and other GPS denied environments. The use of onboard cameras for object tracking and localization [4–9] is a popular way to overcome such shortcomings.

The most challenging phase is the autonomous landing with minimum sensing and computation in the sense that not only does the RUAU have to track a target throughout the maneuver, but both the poses (position and attitude) of the vehicle and the target should also match exactly for successful landing. The task becomes even more challenging if the rotary wing UAV has to track a moving ground vehicle with minimum information while executing the landing maneuver simultaneously [10–21]. A review of various landing techniques can be found in [22, 23]. In [10], landing on a moving target is shown using simple color-based detection and a nonlinear Kalman filter but do not comment on its applicability to target speeds greater than 1 m/s. In [17], a comparative study is carried out between different types of estimators where the vision-based measurements are fused with IMU data for robust localization. The estimators also uses the ground vehicle velocity (with a maximum value of 1.8 m/s) as a state which also aids localization accuracy. A fully autonomous quadrotor system ca-

pable of landing on a moving target using only onboard sensing and computing is demonstrated in [24], but simulations reveal that the efficacy and accuracy of landing directly change significantly with small changes in target speed. In [25], automatic landing of a multirotor UAV on a moving ground vehicle is demonstrated with successful tests executed up to a speed of 50 km/h. However, an extensive sensor suite is used, which is inevitable for any conventional rotorcraft operating at such high speeds. The quadrotor is equipped with a camera with a wide-angle lens pointing downward, an orientable three-axis gimbaled camera for target tracking, and an Inertial Navigation System (INS), while the ground vehicle had a mobile phone on the landing pad which transmitted GPS and IMU data of the ground vehicle to the quadrotor. A similar work with numerous cost intensive sensors can be found in [26] which demonstrates a RUAU system that is capable of landing on a car moving at 15 km/h.

The challenge of landing on a moving target is attributed more so to the under-actuated nature of conventional RUAUs than to the algorithmic components of the landing maneuver. A vehicle, or a system in general, is termed under-actuated when the output degrees of freedom are greater than the input degrees of freedom. A system is termed fully-actuated if the number of input and output degrees of freedom are same [27, Chapter 4]. Most conventional RUAUs are under-actuated with six output degrees of freedom and only four input degrees of freedom. The four inputs are the upward thrust to counteract gravity and the torque inputs responsible for the rolling, pitching, and yawing moments of the vehicle. The horizontal position of the RUAU is controlled by changing the orientation of the vehicle in the inertial frame. The desired orientation (attitude) is achieved by utilizing the torque inputs. Hence, in case of RUAUs, the position and attitude states are coupled. This results in the rotorcraft changing its attitude when trying to move closer to the target, and causes the target to move out of the camera's field of view [28]. The continuous rolling and pitching motion of the RUAU while keeping the target in view and tracking it may result in poor pose estimation and even undesirable behavior at high target velocities [12]. Gimbals are used for image stabilization and controlling the attitude of

the onboard camera when a conventional RUAU is maneuvering [29, 30]. The all-up-weight as well as the overall drag experienced by the UAV increases due to gimbals.

The physical hurdles posed by under-actuation of the UAV can be overcome by augmenting an existing multi-rotor system with additional actuation. A quadrotor with the ability to tilt its rotor tip-path planes increases the number of control inputs of the system from four to eight. However, adding input degrees of freedom changes the dynamics of the vehicle itself. Careful physical modeling of the vehicle dynamics as well as deriving control input expressions has to be carried out. Initial attempts of designing and modeling a tilt-augmented quadrotor were carried out in [31, 32], with emphasis on modeling and dynamics, and provide useful insights. A different quadrotor with rotors tilting about two axes is described in [33]. Using similar models, [34, 35] demonstrate large attitude changes during hover and aggressive maneuvers using differential flatness based control laws are shown in [36]. The existing literature consists of simulation studies with simplified control and actuator allocation without any experimental validation. However, works which present experimental validation use tilt angle feedback with cost-intensive motion capture systems. The present work is an extension of the work done in [37]. The work in [37] focuses on developing an initial prototype, and comparison between conventional and tilt-augmented quadrotors. The present work focuses on developing a more modular tilt-augmented quadrotor and demonstrating its improved abilities for tracking and landing on moving targets using a simple onboard monocular camera. Contributions of the present work are listed in the next subsection.

1.2. Contributions

This paper presents autonomous vision-based tracking and landing on a moving target using a fully-actuated low-cost tilt-augmented quadrotor system. The initial work on modeling of the tilt-augmented quadrotor has been presented in [37]. In this paper the control strategies and control allocation have been improved. Additionally, the major contributions of this work are as follows :

- An adaptive control law that estimates the target velocity and acceleration is presented to track a maneuvering target with only relative position information.
- An extended Kalman filter is utilized to obtain smooth relative pose estimates of the target.
- Trajectories are designed to ensure minimum acceleration during landing which also negates disturbances due to ground effect.
- Low-cost hardware with only IMUs and a monocular camera is used to validate the proposed approach with real-world experiments.

The paper is organized as follows: Section 2 gives a brief overview of the full system. Section 3 presents the full six-degrees of freedom model of the tilt-augmented quadrotor. Section 4 presents a nonlinear control law for attitude stabilization and an adaptive control law for position tracking with minimum information. It also describes the control allocation methodology for the available control inputs and actuators. Section 5 discusses vision-based pose estimation using fiducial markers. Section 6 discusses trajectory generation for landing. Section 7 discusses the numerical simulation and experimental flight test results for tracking and landing. Section 8 summarizes the paper.

2. System Overview

This section provides a brief overview of the components that constitute the overall setup as shown in Fig. 1. Four frames of reference are defined, namely, the inertial (NED) frame (x_i - y_i - z_i), the body frame with its origin coinciding with the vehicle’s center of mass (x_b - y_b - z_b), the camera frame (x_c - y_c - z_c), and the marker frame (x_m - y_m - z_m) which is fixed to the landing platform.

The body frame is defined so that the tilt-augmented quadrotor operates in a “+” configuration. Additional frames of reference are defined for the purpose of expressing the individual rotor thrusts in the body frame due to the presence of tilt-augmentation. The camera frame is fixed with respect to the body frame.

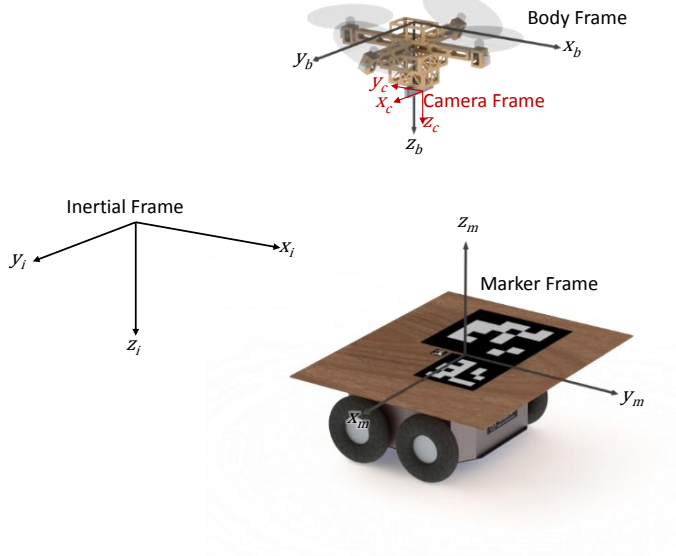


Figure 1: System Overview.

As mentioned earlier, tilt-augmentation eliminates the use of heavy gimbals for pointing and image stabilization at little or no extra cost. Since the roll and pitch angles of both the quadrotor and ground vehicle is constrained to zero, only the yaw angle between the camera and marker frame is used to point the quadrotor in the direction of motion of the ground vehicle. Note that since position tracking can be achieved irrespective of the quadrotor’s yaw angle, the relative yaw error may or may not be zero. When tracking yaw angle of the target is disabled, the yaw angular rate is set to zero so that the quadrotor yaw angle remains constant at the initialized value.

The quadrotor consists of a flight controller, a monocular camera, and an onboard computer for vision-based estimation. The flight controller has an onboard IMU consisting of compass, accelerometers, and gyroscopes. The downward facing camera is used to acquire live feed of the target on the ground. Note that there is no communication between the quadrotor and the ground vehicle. A miniature computer is used for processing the visual data and estimating the

relative position and heading (yaw) of the target with respect to the quadrotor. The ground vehicle is equipped for autonomous as well as manual navigation and carries $1\text{ m} \times 0.8\text{ m}$ platform for landing. Fiducial markers are fixed onto the platform to enable relative pose estimation. Any marker that has features to distinguish the landing pad from its surroundings may be used. ArUco markers [38] are used since pose estimation is simple and not the main focus of this work. Also, use of GPS to provide a rough estimate of the target position is a straightforward extension for long range target tracking. Hence, only the last and most critical stage of vision-based landing is considered in this work for a novel fully-actuated quadrotor. The aforementioned components are described in detail in the coming sections.

3. Quadrotor Modeling

This section presents the dynamic model of the tilt-augmented quadrotor. The model is described in [37] and is included in this work as it forms the basis for subsequent developments and contributions. Attitude kinematics of the vehicle are expressed in terms of quaternions. The rigid body attitude and translational dynamics are derived using Newton's Laws of Motion.

3.1. Reference Frames, Forces, and Moments

A brief summary of the reference frames, forces and moments generated by the quadrotor is given before deriving of the rotational and translational dynamics of the vehicle.

The inertial and the body frames of reference are illustrated in Fig. 1. The forces and rotor angular velocities are shown in Fig. 2. The angular speed of the i^{th} rotor, for $i = 1, 2, 3, 4$, is denoted by ω_i . The magnitudes of thrust and reaction torque generated by the i^{th} rotor is denoted by $F_i = k_f \omega_i^2$ and $M_i = k_m \omega_i^2$, respectively. Here, k_f and k_m are the force and moment coefficients, respectively. Detailed description of these relations can be found in [39, 40]. Since the i^{th} rotor tip-path plane has the ability to rotate about a

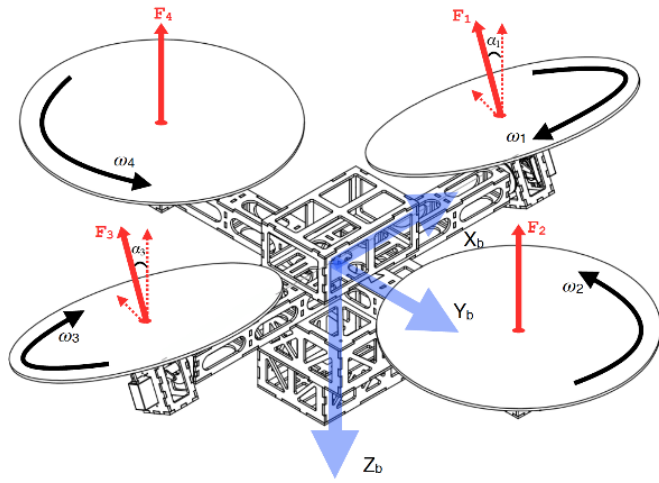


Figure 2: Schematic of the tilt-augmented quadrotor helicopter.

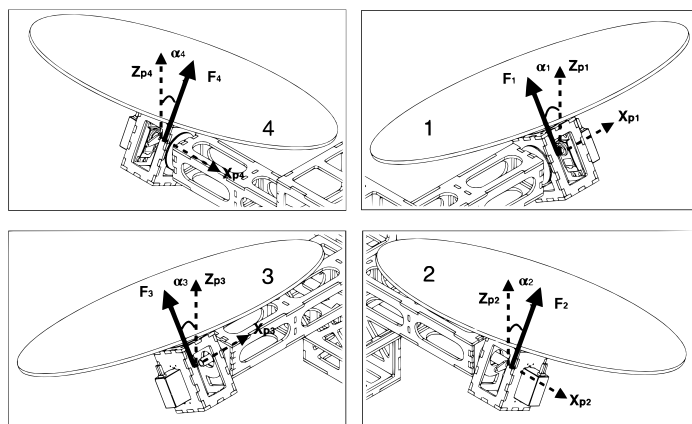


Figure 3: The local propeller frames of reference and tilt angles.

body frame axis, a local fixed propeller frame of reference is defined with the z_{pi} -axis always aligned with the z_b -axis. This is shown in Fig. 3 along with the respective x_{pi} -axes. The associated y_{pi} -axes for a right-handed coordinate system are omitted in the figure to avoid cluttering. The force generated by the i^{th} rotor can be resolved in the respective propeller frame and is given by

$$\mathbf{F}_i = \begin{bmatrix} 0 \\ -k_f \omega_i^2 \sin \alpha_i \\ k_f \omega_i^2 \cos \alpha_i \end{bmatrix}. \quad (1)$$

Similarly, the reaction torque generated by the i^{th} rotor resolved in the respective propeller frame is given by

$$\begin{aligned} \mathbf{M}_i &= \begin{bmatrix} 0 \\ -k_m \omega_i^2 \sin \alpha_i \\ k_m \omega_i^2 \cos \alpha_i \end{bmatrix}, \text{ for } i = 1, 3, \text{ and} \\ \mathbf{M}_i &= \begin{bmatrix} 0 \\ k_m \omega_i^2 \sin \alpha_i \\ -k_m \omega_i^2 \cos \alpha_i \end{bmatrix}, \text{ for } i = 2, 4. \end{aligned} \quad (2)$$

3.2. Attitude Kinematics and Dynamics

The attitude kinematics of the tilt-augmented quadrotor is expressed in terms of unit quaternions. Let $\mathbf{q} \in \mathcal{S}^3$ be an unit quaternion that represents the orientation of the body frame with respect to the inertial frame where the three-dimensional unit sphere is defined as $\mathcal{S}^3 = \{\mathbf{q} \in \mathbb{R}^4 \mid \mathbf{q}^T \mathbf{q} = 1\}$. The quaternion \mathbf{q} is composed of its scalar and vector parts given by $\mathbf{q} = [q_0 \ q_v]^T$, with $q_0 \in \mathbb{R}$ and $q_v \in \mathbb{R}^3$, respectively. From Euler's rotation theorem, any rotation or sequence of rotations of a rigid body can be represented as a single rotation about a fixed axis defined by a vector in \mathbb{R}^3 . Using this, a unit quaternion can be expressed as

$$\mathbf{q} = \left(\cos \left(\frac{\beta}{2} \right), \vec{\eta} \sin \left(\frac{\beta}{2} \right) \right)^T, \quad (3)$$

where $\vec{\eta}$ is the unit vector that represents a fixed axis in \mathbb{R}^3 and β is the amount of rotation about this axis. The quaternion multiplication operation, \circ , for any two quaternions \mathbf{p} and \mathbf{q} is given by

$$\mathbf{p} \circ \mathbf{q} = \begin{bmatrix} p_0 q_0 - p_v^T q_v \\ p_0 q_v + q_0 p_v + p_v \times q_v \end{bmatrix}. \quad (4)$$

The rotation matrix $R(\mathbf{q})$ for a unit quaternion $\mathbf{q} = [q_0 \ q_1 \ q_2 \ q_3]^T$ transforming a vector from the body frame to the inertial frame is then given by

$$R(\mathbf{q}) = \begin{bmatrix} q_0^2 + q_1^2 - q_2^2 - q_3^2 & 2(q_1 q_2 - q_0 q_3) & 2(q_0 q_2 + q_1 q_3) \\ 2(q_1 q_2 + q_0 q_3) & (q_0^2 - q_1^2 + q_2^2 - q_3^2) & 2(q_2 q_3 - q_0 q_1) \\ 2(q_1 q_3 - q_0 q_2) & 2(q_0 q_1 + q_2 q_3) & q_0^2 - q_1^2 - q_2^2 + q_3^2 \end{bmatrix}. \quad (5)$$

The attitude kinematics and dynamics of the vehicle are given by

$$\dot{\mathbf{q}} = \frac{1}{2} \mathbf{q} \circ \boldsymbol{\Omega}, \quad (6a)$$

$$\mathbf{J} \dot{\boldsymbol{\Omega}} = -\boldsymbol{\Omega} \times \mathbf{J} \boldsymbol{\Omega} + \mathbf{M}_b, \quad (6b)$$

where $\boldsymbol{\Omega} \in \mathbb{R}^4$ is the angular velocity quaternion defined as $\boldsymbol{\Omega} = [0 \ \boldsymbol{\Omega}^T]^T$, $\boldsymbol{\Omega} \in \mathbb{R}^3$ is the angular velocity vector of the vehicle expressed in the body frame of reference, $\mathbf{J} = \mathbf{J}^T$ is the positive definite inertia matrix in the body frame, and $\mathbf{M}_b \in \mathbb{R}^3$ is the control input for the rotation dynamics, also defined with respect to the body frame.

For a normal multi-rotor, the control input $\mathbf{M}_b = [M_{b1} \ M_{b2} \ M_{b3}]^T$ on the right side of (6b) is generated by a linear combination of the forces generated by individual rotors. However, due to tilting of the tip-path plane of each rotor, a nonlinear expression arises for each element of \mathbf{M}_b . This is given by

$$\mathbf{M}_b = \sum_{i=1}^4 (\mathbf{l}_i \times R_i^b \mathbf{F}_i) + \sum_{i=1}^4 R_i^b \mathbf{M}_i \quad (7)$$

where \mathbf{l}_i is the displacement of the i^{th} rotor axis from center of mass of the vehicle in the body frame, \mathbf{F}_i is given by (1), and \mathbf{M}_i is given by (2). The rotation matrix R_i^b transforms vectors in the i^{th} propeller frame to the body

frame. These are given by

$$R_i^b = \begin{bmatrix} 1 & 0 & 0 \\ 0 & -1 & 0 \\ 0 & 0 & -1 \end{bmatrix}, \text{ for } i = 1, 3, \quad R_i^b = \begin{bmatrix} 0 & 1 & 0 \\ 1 & 0 & 0 \\ 0 & 0 & -1 \end{bmatrix}, \text{ for } i = 2, 4. \quad (8)$$

Such a nonlinear expression for moment input require careful control allocation which will be explained Section 4.3.

3.3. Translational Dynamics

The translational dynamics of the tilt-augmented quadrotor helicopter in the inertial frame of reference is given by

$$\begin{bmatrix} \ddot{x} \\ \ddot{y} \\ \ddot{z} \end{bmatrix} = \frac{1}{m} R(\mathbf{q}) \mathbf{T}_b + \begin{bmatrix} 0 \\ 0 \\ g \end{bmatrix}, \quad (9)$$

where m denotes mass of the vehicle and g is the acceleration due to gravity. Control input $\mathbf{T}_b = [T_{b1} \ T_{b2} \ T_{b3}]^T$ is defined in the body frame and is given by

$$\mathbf{T}_b = \sum_{i=1}^4 R_i^b \mathbf{F}_i, \quad (10)$$

where R_i^b is defined in (8) and \mathbf{F}_i is given by (1). The ability to tilt the rotor tip-path planes endows the vehicle with additional control inputs along the x_b - and y_b -axes. This also induces cosine terms in the thrust expression along the z_b -axis to counter the gravitational force exerted by the earth as shown in (10).

In a conventional multi-rotor, T_{b1} and T_{b2} are zero since the control input is constrained to be along the z_b -axis by design. This condition of under actuation forces coupling of attitude and position dynamics which is unfavorable in terms of control design as well as carrying payloads. From (7) and (10), it is observed that there are individual control inputs for all six degrees of freedom of the vehicle. This enables us to think of control design for each degree of freedom separately with appropriate allocation.

4. Control Design and Allocation

In this section, nonlinear control laws for attitude and position of the tilt-augmented quadrotor are presented. The attitude control law uses quaternions for simplicity. An adaptive position control law is derived that estimates the ground target's acceleration using only the relative position measurements. The adaptive control law is required since the Kalman filter that is used for vision-based localization can only estimate relative position, velocity and acceleration and not the target velocity and acceleration.

4.1. Attitude Control

Attitude control of under-actuated quadrotors using quaternions is described in [41, 42]. In this work, the tilt-augmented quadrotor is required to track a quaternion of the form

$$\mathbf{q}_d = \left(\cos\left(\frac{\psi}{2}\right), 0, 0, \sin\left(\frac{\psi}{2}\right) \right)^T, \quad (11)$$

where \mathbf{q}_d is the desired quaternion and ψ is the heading or yaw angle of the target. This is because the tilt-augmented quadrotor should stabilize its roll and pitch angles to zero at all times while having the option to track a heading command coming from the estimated target pose. The attitude quaternion error is defined as

$$\mathbf{q}_e = \mathbf{q}_d^* \circ \mathbf{q}, \quad (12)$$

where $\mathbf{q}_d^* = [q_0 \ -q_v^T]^T$ denotes the conjugate or inverse of the desired quaternion and $\mathbf{q}_e = [q_{0e} \ q_{ve}^T]^T$ is the error quaternion in terms of its scalar and vector parts. The error quaternion computed in (12) represents the proportional attitude error. For attitude stabilization case, the desired angular velocity vector, denoted by Ω_d , is taken to be the origin of \mathbb{R}^3 . The control law utilized for attitude stabilization is given by [37]

$$\mathbf{M}_b = -K_q q_{0e} q_{ve} - K_\Omega \Omega, \quad (13)$$

where $K_q, K_\Omega \in \mathbb{R}^{3 \times 3}$ are positive definite diagonal matrices. Detailed stability proof of the above attitude control law with non-zero Ω_d can be found in [43].

4.2. Position Control

The position tracking performance of linear controllers like PID when only relative position error is known can be improved only up to a certain extent. The derivative term helps enhance the transient response but the bandwidth is limited due to high frequency noise. Recent surveys show extensive use of non-linear adaptive controllers for trajectory tracking using conventional quadrotors [44, 45]. However, most works concentrate on developing adaptive and robust controllers for overcoming modeling uncertainties, robustness to disturbances, and for handling cases of rotor failure. Moreover, the aforementioned works along with those found in [46, 47] deal with control of conventional RUAVs. To the best of the authors' knowledge, none of the previous works have utilized the idea of an adaptive control law to estimate target acceleration and velocity for a tilt-augmented quadrotor.

For UAV position control in this work, a feed-forward term is included to improve the tracking performance of the controller. However, the feed-forward term, which is the desired acceleration, is unavailable in our system as no *a priori* information about the movement of the ground vehicle is known. Also, no communication exists between the ground vehicle and the **RUAV**. Acceleration and velocity estimates from vision-based systems are extremely unreliable and inaccurate even with nonlinear Kalman filters or linear/nonlinear observers. This is because vision-based localization only provides the relative position information with good accuracy. Therefore, an adaptive control technique is used for position control to stabilize as well as estimate the reference derivatives.

Modifying (9) by replacing the term $R(\mathbf{q})\mathbf{T}_b$ with a vector $\mathbf{U} = [u_1 \ u_2 \ u_3]^T$, a simplified form of the dynamics is given by

$$\begin{bmatrix} \ddot{x} \\ \ddot{y} \\ \ddot{z} \end{bmatrix} = \frac{1}{m} \begin{bmatrix} u_1 \\ u_2 \\ u_3 \end{bmatrix} + \begin{bmatrix} 0 \\ 0 \\ g \end{bmatrix}. \quad (14)$$

Let $\mathbf{g} = [0 \ 0 \ g]^T$ be the gravity vector, $\mathbf{x}_1 = [x \ y \ z]^T$ be the position vector, $\mathbf{x}_2 = [\dot{x} \ \dot{y} \ \dot{z}]^T$ be velocity vector, and \mathbf{U} be the control vector or the

forces exerted by the four rotors with tilt-augmentation in the inertial frame. The position, velocity, and acceleration references are denoted by the vectors \mathbf{r} , $\dot{\mathbf{r}}$, and $\ddot{\mathbf{r}}$, respectively. The mass of quadrotor, m , and the gravity vector, \mathbf{g} , are assumed to be constant. The second order translational dynamics of the tilt-augmented quadrotor can now be written in the strict-feedback form as

$$\begin{aligned}\dot{\mathbf{x}}_1 &= \mathbf{x}_2, \\ \dot{\mathbf{x}}_2 &= \mathbf{g} + \frac{1}{m}\mathbf{U}.\end{aligned}\tag{15}$$

For designing a tracking controller, the errors in position and velocity are defined as $\mathbf{e}_1 = \mathbf{x}_1 - \mathbf{r}$ and $\mathbf{e}_2 = \mathbf{x}_2 - \dot{\mathbf{r}}$, respectively. The error dynamics can be written as

$$\begin{aligned}\dot{\mathbf{e}}_1 &= \mathbf{e}_2, \\ \dot{\mathbf{e}}_2 &= \mathbf{g} + \frac{\mathbf{U}}{m} + \boldsymbol{\theta}_a,\end{aligned}\tag{16}$$

where $\boldsymbol{\theta}_a = -\ddot{\mathbf{r}}$ is to be estimated. For stability analysis that follows, the estimation error is defined as $\tilde{\boldsymbol{\theta}}_a = \boldsymbol{\theta}_a - \hat{\boldsymbol{\theta}}_a$, where $\hat{\boldsymbol{\theta}}_a$ is an estimate of $\boldsymbol{\theta}_a$. The relative velocity estimates of the target using the Kalman filter running onboard for vision-based localization gives noisy estimates that leads to undesirable closed-loop behavior. Thus, the reference velocity is also estimated using integration of the acceleration estimate. Estimation of the target velocity directly, rather than using the relative velocity estimate, also allows the use of the onboard quadrotor velocity estimate to compute the estimated velocity error, $\hat{\mathbf{e}}_2$. The quadrotor velocity is estimated by the EKF running onboard the autopilot which uses IMU measurements. This estimate is more reliable and is much less noisy as compared to obtaining the relative velocity through differentiation. Let the target velocity be denoted by $\boldsymbol{\theta}_v = -\dot{\mathbf{r}}$. The estimation error is defined as $\tilde{\boldsymbol{\theta}}_v = \boldsymbol{\theta}_v - \hat{\boldsymbol{\theta}}_v$, where $\hat{\boldsymbol{\theta}}_v$ is an estimate of $\boldsymbol{\theta}_v$. It should be noted that $\boldsymbol{\theta}_a$, $\hat{\boldsymbol{\theta}}_a$, and $\tilde{\boldsymbol{\theta}}_a$ are essentially the derivatives of $\boldsymbol{\theta}_v$, $\hat{\boldsymbol{\theta}}_v$, and $\tilde{\boldsymbol{\theta}}_v$, respectively. The estimated velocity error, $\hat{\mathbf{e}}_2$, is defined as

$$\hat{\mathbf{e}}_2 = \mathbf{x}_2 + \hat{\boldsymbol{\theta}}_v = \mathbf{x}_2 + \int_0^t \hat{\boldsymbol{\theta}}_a(\tau) d\tau.\tag{17}$$

Since $\ddot{\mathbf{r}}$ and $\dot{\mathbf{r}}$ are not known *a priori*, the approximated dynamics equation for \mathbf{e}_2 used for control design, is given by differentiating (17) as

$$\dot{\hat{\mathbf{e}}}_2 = \mathbf{g} + \frac{\mathbf{U}}{m} + \hat{\boldsymbol{\theta}}_a, \quad (18)$$

Thus, from the definition of \mathbf{e}_2 and (17), the expression for $\tilde{\boldsymbol{\theta}}_v$ comes out to be

$$\tilde{\boldsymbol{\theta}}_v = \mathbf{e}_2 - \hat{\mathbf{e}}_2, \quad (19)$$

and its derivative is given by

$$\dot{\tilde{\boldsymbol{\theta}}}_v = \dot{\mathbf{e}}_2 - \dot{\hat{\mathbf{e}}}_2 = \tilde{\boldsymbol{\theta}}_a. \quad (20)$$

The equilibrium of error dynamics in (16), (18), and (20) turns out to be

$$\mathbf{e}_1^{id} = \frac{\boldsymbol{\theta}_a}{\gamma}, \quad \hat{\mathbf{e}}_2^{id} = -\frac{K_p \boldsymbol{\theta}_a}{\gamma K_v}, \quad \text{and} \quad \tilde{\boldsymbol{\theta}}_v^{id} = \frac{K_p \boldsymbol{\theta}_a}{\gamma K_v}, \quad (21)$$

where K_p , K_v , and γ are real positive finite constants.

Theorem 1. *For the error dynamics given in (16) and (18), with real positive finite constants K_p , K_v , and γ , the control law given by*

$$\mathbf{U} = m \left(-\mathbf{g} - K_p \mathbf{e}_1 - K_v \hat{\mathbf{e}}_2 - \hat{\boldsymbol{\theta}}_a \right), \quad (22)$$

with the parameter estimation law given by

$$\dot{\tilde{\boldsymbol{\theta}}}_v = \hat{\boldsymbol{\theta}}_a = \gamma \mathbf{e}_1, \quad (23)$$

- (i) *globally asymptotically stabilizes the identity element of the error space,*
 $(\mathbf{e}_1^{id}, \hat{\mathbf{e}}_2^{id}, \tilde{\boldsymbol{\theta}}_v^{id}) \equiv (0_{3 \times 1}, 0_{3 \times 1}, 0_{3 \times 1})$, if $\ddot{\mathbf{r}} = 0$.
- (ii) *ensures that the errors remain bounded for all time, if $\ddot{\mathbf{r}} \neq 0$ and $\ddot{\mathbf{r}}$ is a finite constant.*

Proof. Consider a Lyapunov candidate function given by

$$V = \frac{K_p}{2} (\mathbf{e}_1 - \mathbf{e}_1^{id})^T (\mathbf{e}_1 - \mathbf{e}_1^{id}) + \frac{1}{2} (\hat{\mathbf{e}}_2 - \hat{\mathbf{e}}_2^{id})^T (\hat{\mathbf{e}}_2 - \hat{\mathbf{e}}_2^{id}) + \frac{K_p}{2\gamma} (\tilde{\boldsymbol{\theta}}_v - \tilde{\boldsymbol{\theta}}_v^{id})^T (\tilde{\boldsymbol{\theta}}_v - \tilde{\boldsymbol{\theta}}_v^{id}). \quad (24)$$

The function V is positive definite and the time derivative of V is given by

$$\dot{V} = K_p(\mathbf{e}_1 - \mathbf{e}_1^{id})^T \dot{\mathbf{e}}_1 + (\hat{\mathbf{e}}_2 - \hat{\mathbf{e}}_2^{id})^T \dot{\hat{\mathbf{e}}}_2 + \frac{K_p}{\gamma}(\tilde{\boldsymbol{\theta}}_v - \tilde{\boldsymbol{\theta}}_v^{id})^T \dot{\tilde{\boldsymbol{\theta}}}_v. \quad (25)$$

Substituting (16), (18), (19), and (20) in (25), the expression for \dot{V} is written as

$$\dot{V} = K_p(\mathbf{e}_1 - \mathbf{e}_1^{id})^T \mathbf{e}_2 + (\hat{\mathbf{e}}_2 - \hat{\mathbf{e}}_2^{id})^T (\mathbf{g} + \frac{\mathbf{U}}{m} + \hat{\boldsymbol{\theta}}_a) + \frac{K_p}{\gamma}(\mathbf{e}_2 - \hat{\mathbf{e}}_2 - \tilde{\boldsymbol{\theta}}_v^{id})^T \tilde{\boldsymbol{\theta}}_a. \quad (26)$$

Using (21), (22), and (23),

$$\dot{V} = -\hat{\mathbf{e}}_2^T K_v \hat{\mathbf{e}}_2 + \hat{\mathbf{e}}_2^{id^T} K_v \hat{\mathbf{e}}_2^{id} = -K_v \|\hat{\mathbf{e}}_2\|^2 + K_v \|\hat{\mathbf{e}}_2^{id}\|^2, \quad (27)$$

where $\|\cdot\|$ is the 2-norm defined on \mathbb{R}^n .

- (i) For $\vec{r} = 0$, $\hat{\mathbf{e}}_2^{id} = 0$. Hence, $\dot{V} \leq 0$ over the complete error space. Thus, $\mathcal{P}_1 = \left\{ (\mathbf{e}_1^{id}, \hat{\mathbf{e}}_2^{id}, \tilde{\boldsymbol{\theta}}_v^{id}) \right\}$ is the largest invariant set in the complete error space. Global asymptotic stabilization of the equilibrium $(\mathbf{e}_1^{id}, \hat{\mathbf{e}}_2^{id}, \tilde{\boldsymbol{\theta}}_v^{id})$ in the error space using the control law in (22) follows from *LaSalle's Invariance Principle*.
- (ii) For $\vec{r} \neq 0$, $\dot{V} \leq 0$ whenever $\|\hat{\mathbf{e}}_2\|^2 \geq \|\hat{\mathbf{e}}_2^{id}\|^2$. For $\|\hat{\mathbf{e}}_2\| \leq \|\hat{\mathbf{e}}_2^{id}\|$, define a set $\mathcal{P}_{\varepsilon_1} = \left\{ (\mathbf{e}_1, \hat{\mathbf{e}}_2, \tilde{\boldsymbol{\theta}}_v) : V \leq \varepsilon_1 \right\}$, where $\varepsilon_1 > 0$. From (17), (19), and (23), assuming finite quadrotor and target velocities, the errors \mathbf{e}_1 and $\tilde{\boldsymbol{\theta}}_v$ are bounded inside the set $\mathcal{P}_{\varepsilon_1}$. In other words, there exist errors $\mathbf{e}_1^{\mathcal{P}max}$, $\tilde{\boldsymbol{\theta}}_v^{\mathcal{P}max} \in \mathcal{P}_{\varepsilon_1}$ such that

$$\|\mathbf{e}_1\| \leq \|\mathbf{e}_1^{\mathcal{P}max}\|, \|\hat{\mathbf{e}}_2\| \leq \|\hat{\mathbf{e}}_2^{id}\|, \|\tilde{\boldsymbol{\theta}}_v\| \leq \|\tilde{\boldsymbol{\theta}}_v^{\mathcal{P}max}\|,$$

where $\|\mathbf{e}_1^{\mathcal{P}max}\|, \|\tilde{\boldsymbol{\theta}}_v^{\mathcal{P}max}\| < \infty$, $\forall \mathbf{e}_1, \hat{\mathbf{e}}_2, \tilde{\boldsymbol{\theta}}_v \in \mathcal{P}_{\varepsilon_1}$. Hence, $\mathcal{P}_{\varepsilon_1}$ is compact and all solutions starting inside this set remain there for all future time. Outside $\mathcal{P}_{\varepsilon_1}$, $\dot{V} < 0$. This ensures that the tracking errors are uniformly ultimately bounded. Since V is radially unbounded, the result is valid globally.

□

The vector $\mathbf{U} \in \mathbb{R}^3$ is the control input defined in the inertial frame of reference and is given by (22). Hence, it has to be transformed into the body frame of reference. This is given by

$$\mathbf{T}_b = R(\mathbf{q})^T \mathbf{U}. \quad (28)$$

Note that this transformation of the desired control input vector in the inertial frame to the body frame uses the current rotation matrix and is done to preserve consistency of the reference frames used.

4.3. Control Allocation

The control allocation for a tilt-augmented quadrotor has been discussed previously in [37]. Recent literature on tilt-augmented multirotors show that it is highly difficult to allocate controls for over-actuated systems, especially without feedback of the variables used for actuation [48]. The use of pseudo-inverse based methods lead to multiple non-feasible solutions which is not desirable [48]. Even in the case of fully-actuated RUAVs, aggressive attitude tracking while independently achieving position tracking is impossible without tilt-angle measurements [34, 35]. Hence, a more reliable methodology for control allocation on the lines of [37] is utilized in this work. The actuators for each system degree of freedom is decided beforehand based on (7) and (10). The control allocation utilized allows position tracking while stabilizing roll and pitch of the vehicle with only minimal state estimation similar to conventional quadrotors. To ensure control along z_b -axis using upward total thrust is not lost at any stage of flight, a limit of $\alpha_i \leq \pm 60^\circ$ is imposed. This value is derived from the fact that a rotorcraft, in general, is designed to produce an upward thrust that is twice its all-up-weight. It also enables the use of low-cost servos for the tilting mechanism which, in general, have an operating range of $\pm 90^\circ$.

The direct linear allocation given in [37] is however valid only for a small region of operation and with linear position control laws. Exceedingly simple allocation for the height control input loses the scaling information of the force coefficient, k_f . This in turn increases the difficulty in tuning the gains in (22).

Hence, the rotor speed allocation is done analogous to conventional quadrotors. Since rotor speeds are also used for attitude stabilization, control allocation of \mathbf{M}_b and T_{b3} to ω_i , for $i = 1, 2, 3, 4$, is done as follows :

$$\begin{bmatrix} \omega_1^2 \\ \omega_2^2 \\ \omega_3^2 \\ \omega_4^2 \end{bmatrix} = \begin{bmatrix} k_f & k_f & k_f & k_f \\ 0 & -l k_f & 0 & l k_f \\ l k_f & 0 & -l k_f & 0 \\ -k_m & k_m & -k_m & k_m \end{bmatrix}^{-1} \begin{bmatrix} T_{b3} \\ M_{b1} \\ M_{b2} \\ M_{b3} \end{bmatrix}. \quad (29)$$

Given the constraint on tilt angles, and the control input expressions for \mathbf{M}_b and T_{b3} , this type of control allocation is feasible.

Since the tilt-augmented quadrotor has eight actuators due to tilting rotors, the conditions $\alpha_1 = \alpha_3$ and $\alpha_2 = \alpha_4$ are added to ensure the vehicle is fully-actuated. To assign the control inputs T_{b1} and T_{b2} to the tilt angles, the following expression is utilized :

$$\begin{bmatrix} \alpha_1 \\ \alpha_2 \end{bmatrix} = \begin{bmatrix} 0 & 0.5 \\ -0.5 & 0 \end{bmatrix} \begin{bmatrix} T_{b1} \\ T_{b2} \end{bmatrix}. \quad (30)$$

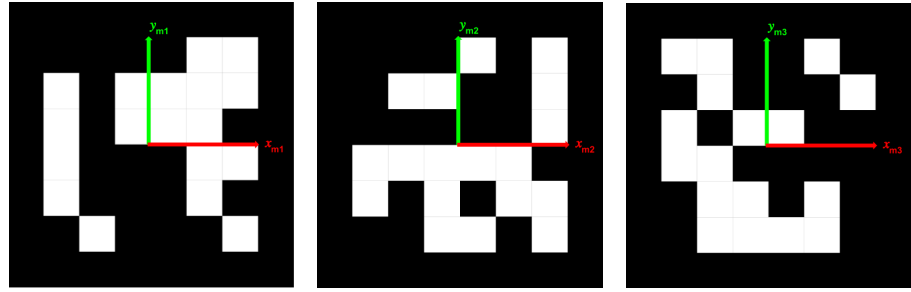
The tilt angle allocation given in [37] cannot be directly used for improved position tracking using feed-forward terms given in (22). This is because the terms in the matrix on the right hand side of (30) act as weights for the tilt angles. Hence, larger the weight, larger is the rotor tilt, for a fixed control input. Therefore, the weights have to be chosen carefully in accordance with the control law used as well as the maneuvers required in the $x_i - y_i$ plane. A lower weight is chosen in this work since there is an additional feed-forward term appearing in (22) which changes the closed-loop response of the system significantly. [Hence, these weights can be used as tuning parameters while using different control laws.](#)

In the next section, vision-based estimation of relative pose is described. The relative position of the quadrotor with respect to the marker gives the position error which is used by the position controller.

5. Vision-based Localization

The relative localization of quadrotor is done using ArUco marker detection suite [49] in OpenCV [50]. The method provides the full relative pose of the camera with respect to the marker. This means that the relative position vector and the attitude in terms of a quaternion are extracted. However, for a given size of the marker, the measurement becomes noisy and unreliable when the marker is far away from the camera. This scenario occurs when using a marker which is small enough to be detected even after the quadrotor has landed. Noise in the measured pose increases with distance since estimation of the marker size becomes difficult at larger distances. In order to have a smooth landing on the platform, a set of three markers of successively decreasing size is used to provide the localization information. Size of the largest marker is chosen to give reliable data at a reasonable distance from the landing platform. The pose estimate from the largest marker visible is used and hence smallest localization error is achieved. As the quadrotor descends, the largest marker becomes truncated and the algorithm automatically switches over to the next largest marker for localization. The size of the smallest and the largest markers are chosen based on the closest and farthest approach to the platform at which the localization information is needed for landing. The intermediate marker size is decided so as to ensure a smooth landing trajectory. The markers used are shown in Fig. 4 and the compound marker is shown in Fig. 5.

Note that each marker has its own individual marker frame (all frames follow right-handed convention) and origin associated with it as denoted in Fig. 4. To avoid jerks while transitioning from one marker to another during the landing phase, a single origin for the compound marker frame is defined. Since the smallest marker is in view even after the quadrotor has landed, the origin of the compound marker is chosen to coincide with that of the smallest marker. The origins of the remaining markers are shifted accordingly using the transformations given in (31). The rotation matrix $R_{M_n}^c$ transforms vectors in the n^{th} marker frame to the camera frame while the rotation matrix $R_c^{M_n} = (R_{M_n}^c)^T$



(a) Marker 1 (M_1, \mathcal{O}_1 , Smallest). (b) Marker 2 (M_2, \mathcal{O}_2 , Second largest). (c) Marker 3 (M_3, \mathcal{O}_3 , Largest).

Figure 4: Markers used to construct the compound marker.

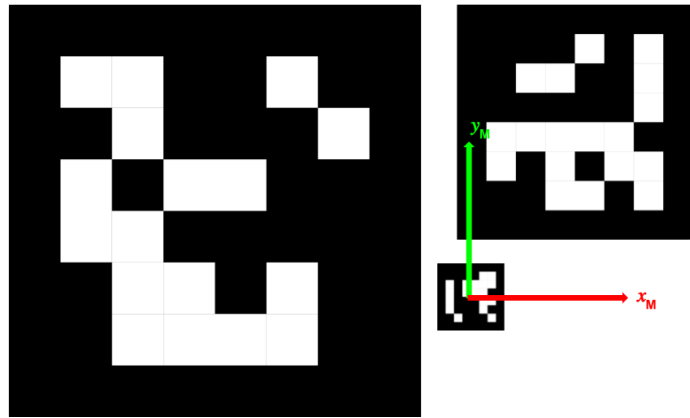


Figure 5: Compound marker used for landing. Size of marker 3 is $0.405 \text{ m} \times 0.405 \text{ m}$, size of marker 2 is $0.250 \text{ m} \times 0.250 \text{ m}$, and size of marker 1 is $0.050 \text{ m} \times 0.050 \text{ m}$.

transforms vectors in the camera frame to the n^{th} marker frame. The position vector of \mathcal{O}_1 given in marker frame \mathcal{M}_n is $\text{offset}_n^1 \in \mathbb{R}^3$ for $n = 2, 3$. The rotation matrix, $R_{M_n}^c$, is computed from the quaternion obtained from the relative attitude measurement.

$$\mathcal{O}_2^{\text{offset}} = R_{M_2}^c (R_c^{M_2} \mathcal{O}_2 + \text{offset}_2^1) = \mathcal{O}_1, \quad (31\text{a})$$

$$\mathcal{O}_3^{\text{offset}} = R_{M_3}^c (R_c^{M_3} \mathcal{O}_3 + \text{offset}_3^1) = \mathcal{O}_1. \quad (31\text{b})$$

The ArUco marker detection node is running on the onboard computer at 20 Hz and the position controller on the flight controller is running at 30 Hz. Such discontinuities in the measurements are undesirable. Hence, a Kalman filter, also running at 30 Hz, has been deployed to smoothen out the raw measurements and act as a buffer. It also provides predictions in case the detection fails due to blurriness during the movement of the quadrotor or the marker. A simple implementable model [51] is adopted to suit the present work. [Since the Kalman filter model is fairly standard and well known, the details are skipped.](#)

Once the filtered compound marker pose is estimated in the camera frame, the vectors in the camera frame have to be transformed first into the quadrotor body frame and then into the inertial frame. For a conventional quadrotor with a gimbal attached for camera stabilization, this matrix is not a constant and has to be continuously estimated. This adds to the computational cost and still does not solve the problem of the quadrotor rolling and pitching when it is about to land on a moving target. For a tilt-augmented quadrotor where the camera is rigidly fixed as shown in Fig. 1, the rotation matrix from the camera frame to the body frame, R_c^b , is given by

$$R_c^b = \begin{bmatrix} 0 & -1 & 0 \\ 1 & 0 & 0 \\ 0 & 0 & 1 \end{bmatrix}. \quad (32)$$

Finally, the rotation matrix from the quadrotor body frame to the inertial frame, R_b^i , is estimated using an EKF that is running on the flight controller.

6. Landing Trajectory Generation

The height setpoints for the landing maneuver are generated using a combination of minimum acceleration trajectory and a conical safe landing zone. A differential flatness approach similar to that in [52] is followed. The trajectories are generated only in the z_i direction as the adaptive controller is sufficient only for tracking the moving ground vehicle in the $x_i - y_i$ plane and counteract any ground effect during landing. The trajectories are optimized for minimum acceleration as the control input occurs in the second derivative of the flat outputs as is evident in (9). Since the translational and rotational dynamics are decoupled due to tilt-augmentation, the higher derivatives of position like snap need not be considered which is typically done for conventional quadrotors.

The optimization of the trajectory is done by minimizing the second derivative of position over the duration of the trajectory. In other words, a quadratic cost functional is minimized given by

$$J = \int_{t_0}^{t_f} \|\ddot{r}_3(t)\|^2 dt, \quad (33)$$

where r_3 is the z -component of the reference position. To get the necessary condition for minimum acceleration, basic Euler-Lagrange equations are utilized which are given by

$$\frac{\partial \mathcal{L}}{\partial f} + \sum_{k=1}^n (-1)^k \frac{d^k}{dt^k} \frac{\partial \mathcal{L}}{\partial f^{(k)}} = 0, \quad (34)$$

where $f^{(k)}$ denotes the k^{th} derivative with respect to time of some function f .

For the flat output r_3 ,

$$f = r_3 \quad \text{and} \quad \mathcal{L} = (\ddot{r}_3)^2,$$

yielding

$$r_3^{(4)} = 0. \quad (35)$$

This indicates that a third order polynomial for height reference will satisfy the necessary conditions and generate the optimal trajectory given the appropriate boundary conditions. A polynomial trajectory can be defined as $\mathbf{b}^T \mathbf{c}$ where

\mathbf{b} contains the basis $\mathbf{b} = [1 \ t \ t^2 \ t^3]^T$ and \mathbf{c} contains the coefficients $\mathbf{c} = [c_0 \ c_1 \ c_2 \ c_3]^T$. The coefficients can be efficiently generated by inverting a single matrix of basis vectors and multiplying it with the boundary constraints as given by

$$\mathbf{c} = \begin{bmatrix} \mathbf{b}(t_0)^T \\ \dot{\mathbf{b}}(t_0)^T \\ \mathbf{b}(t_f)^T \\ \dot{\mathbf{b}}(t_f)^T \end{bmatrix}^{-1} \begin{bmatrix} r_3(t_0) \\ \dot{r}_3(t_0) \\ r_3(t_f) \\ \dot{r}_3(t_f) \end{bmatrix}, \quad (36)$$

where t_0 and t_f are the initial time and final time, respectively. The boundary conditions for the landing maneuver are given in Table 1. The final velocity is some positive value to counteract the ground effect during the final stages of landing and to lessen the duration in which the quadrotor hovers in ground effect.

Table 1: Boundary conditions for landing trajectory generation.

Time	Position (z_i -axis)	Velocity (z_i -axis)
t_0	$r_3(t_0)$	$\dot{r}_3(t_0)$
t_f	$r_3(t_f)$	$\dot{r}_3(t_f)$

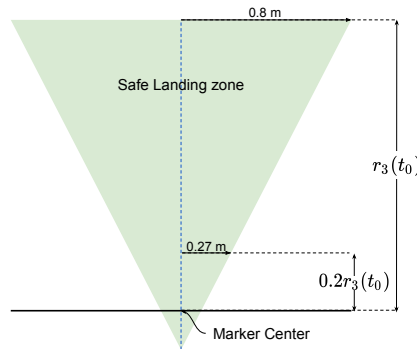


Figure 6: Conical safe landing zone. The error bounds of 0.8 m and 0.27 m are specified for the case where $r_3(t_0) = 1.5$ m.

The complete landing maneuver is designed with the idea of precision landing. Therefore, the quadrotor must satisfy some bounds in the $x_i - y_i$ plane during landing which is dependent on the desired landing precision and the onboard camera's field of view. Besides, some unforeseen disturbances may occur during landing that might result in a large change of the quadrotor position or attitude. To address all these issues, a fail-safe is introduced in the height setpoint generator that will reset the landing maneuver if the fail-safe is activated. For precision landing, a safe landing zone is defined that is shaped like an inverted cone with the marker at the center as shown in Fig. 6. Within this conical zone, the height setpoints from the landing trajectory will be provided to the position controller. If the quadrotor moves out of this safe zone, the landing maneuver is reset. As a result the starting time of the trajectory generator is reset to the current time. The quadrotor hence moves up to the starting position of the trajectory at $t = t_0$.

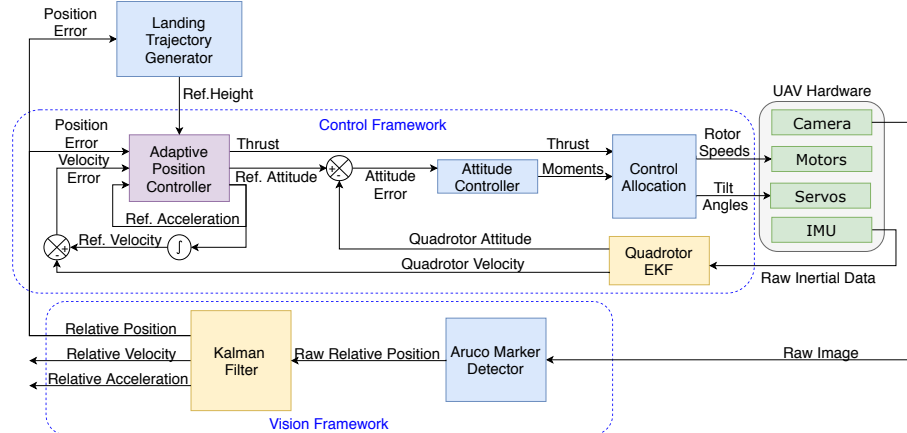


Figure 7: Block diagram of the tilt-augmented quadrotor.

The block diagram representation of the overall architecture is shown in Fig. 7. The raw image is processed by the ArUco marker detector to give the relative pose measurements in the camera frame. The Kalman filter running on the miniature computer onboard provides filtered estimate of the relative pose in the inertial frame of reference. The adaptive position controller uses

this information along with the height setpoints from the landing trajectory generator to estimate the target acceleration and executes the landing maneuver. The attitude controller ensures the quadrotor is stabilized at zero roll and pitch angle throughout the flight. Optionally, the heading (yaw) can be supplied from the pose measurement to enable the quadrotor to have identical heading as the ground vehicle. The control allocation given in (29) and (30) ensures that the rotor speeds and tilt angles are supplied to the appropriate actuators.

7. Results

This section presents the experiments both in simulation and in the real-world. Simulations are done to validate the proposed control laws as well as the overall methodology. Real-world experiments are performed to validate the proposed architecture for tracking and landing on a moving target with only a low-cost sensor suite consisting of an onboard monocular camera and IMUs. These results, along with the experimental setup used, are presented below.

Table 2: Parameters of the tilt-augmented quadrotor used for simulations and experiments.

Parameter (Unit)	Value
Mass (kg)	3.0
Inertia about x_b -axis (kg m^2)	0.03
Inertia about y_b -axis (kg m^2)	0.03
Inertia about z_b -axis (kg m^2)	0.06

7.1. Simulation Results

Numerical simulations are carried out in MATLAB and presented to show the effectiveness of the proposed control methodology. It is shown that the adaptive control law for the translational dynamics works much better than traditional PID controllers in the case of moving targets when only relative position information is available. Constant velocity, constant acceleration, and

sinusoids are given to the position controller as reference signals. Gaussian noise of mean zero and covariances 0.02 m in position, 0.01 m/s in velocity, and 0.1° in each servo tilt angle are added. The noise covariances considered for simulations are much higher than those obtained experimentally. The rate of change of servo angle is limited to 90°/s. The maximum thrust provided by each rotor is half of the all-up-weight of the quadrotor. The tilt angles are restricted between $\pm 60^\circ$. The quadrotor parameters used for simulations are given in Table 2. Results show the superior performance of the adaptive control law. The attitude controller is unchanged for both cases and plots are given for completeness.

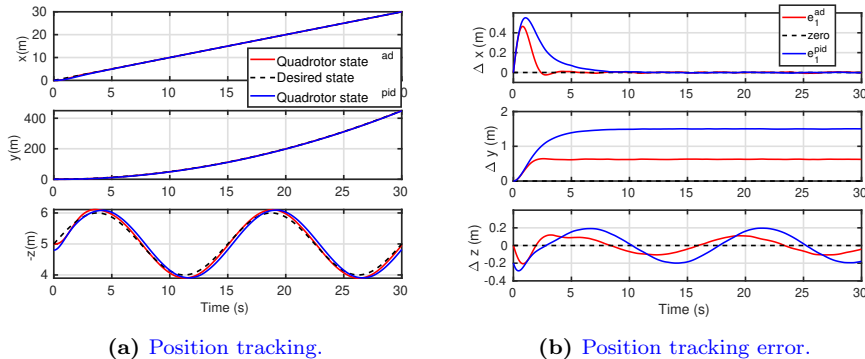


Figure 8: Position tracking and tracking error comparison between adaptive and PID controllers. Both controllers do not have any desired velocity and acceleration information.

Table 3: Reference signals used for controller performance comparison.

Axis	Reference signal
x_i -axis	Constant velocity of 1 m/s
y_i -axis	Constant acceleration of 1 m/s ²
z_i -axis	Sinusoid of magnitude 1 m and time period 15 s

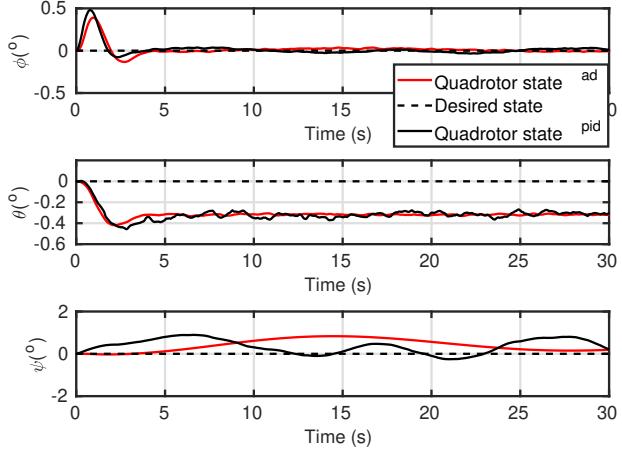


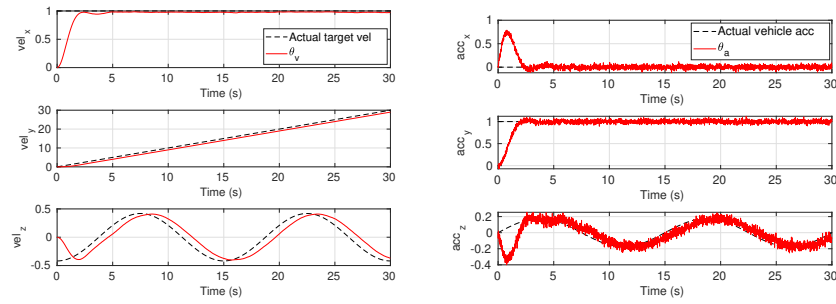
Figure 9: Attitude tracking using the control law given in (13). The superscripts indicating adaptive and PID controllers refer to the position controllers running correspondingly. It can be observed that the attitude is virtually unchanged even during position tracking.

Figure 8a shows the position tracking of the proposed adaptive control law as well as the traditional PID controller. The control allocation given in [37] is used with the PID controller to ensure good tracking performance. The reference signals used are given in Table 3.

Both the controllers do not have any information about the target velocity and target acceleration. Controller gains are chosen to ensure the best possible closed-loop response. For the adaptive case, $K_p = 1.8$, $K_v = 1.0$, $\gamma = 1.5$. The proportional, integral, and derivative gains were taken to be 5.0, 0.01, and 3.0, respectively. The error plots are given in Fig. 8b. It is observed that the adaptive control law performs much better than PID. The roll, pitch, and yaw angles illustrated in Fig. 9 show that attitude changes are minimal. The attitude controller gains are $K_q = \text{diag}(1.5 \ 1.5 \ 1.5)$ and $K_\Omega = \text{diag}(0.3 \ 0.3 \ 0.3)$. Euler angles for roll, pitch, and yaw (ϕ , θ , and ψ , respectively) are plotted for easy visualization since they are more intuitive.

The velocity and acceleration estimates are given in Fig. 10a and Fig. 10b, respectively. The tilt angles for both cases are plotted in Fig. 11. Since the

condition $\alpha_1 = \alpha_3$ and $\alpha_2 = \alpha_4$ is true, only α_1 and α_2 are plotted for both cases. The tilt angles are within bounds for both the adaptive controller case as well as the PID case. However, a larger tilt can be observed initially for α_2^{ad} as compared to α_2^{pid} . This implies a larger force is applied to track a step change in velocity along the x_i -axis and hence error goes to zero faster in the case of adaptive control law as seen in Fig. 8b.



(a) Velocity estimate, θ_v , and reference velocity, \dot{r} . (b) Acceleration estimate, θ_a , obtained from (23) and reference acceleration, \ddot{r} .

Figure 10: Velocity and acceleration estimates. (a) The velocity estimate converges quickly to the actual value of the desired velocity for the constant velocity case. (b) The acceleration estimate is observed to converge to its true value.

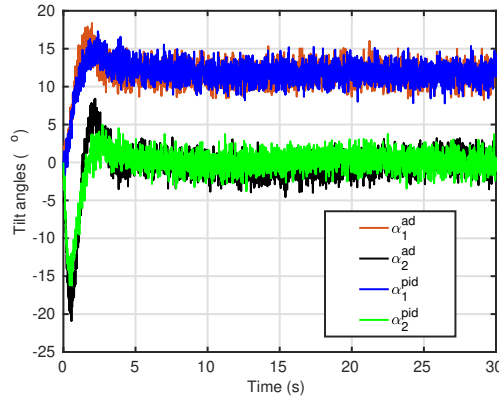


Figure 11: Tilt angles for the tracking simulation. The adaptive control law performs better than PID since it uses velocity and acceleration estimates to improve its tracking.

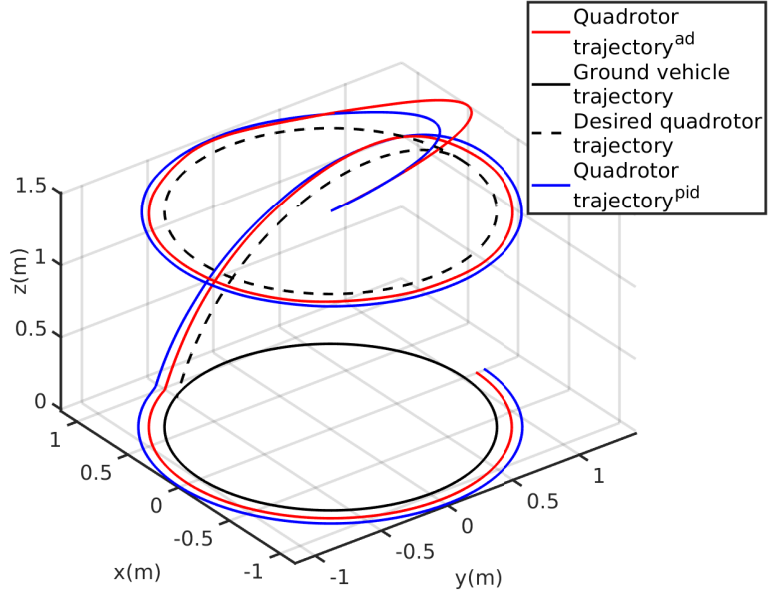


Figure 12: Landing on a moving target. The trajectories indicate that tracking performance of the adaptive control law is better than that of the PID controller. Since the error is lesser, the landing maneuver is more precise. This reduces the risk of failure.

Landing on a target moving in a circle is simulated next. The three-dimensional plot of the quadrotor trajectory using the adaptive control law and PID controller is shown in Fig. 12. The desired trajectories along x_i - and y_i -axes are given as $\sin(\frac{2\pi}{15}t)$ and $\cos(\frac{2\pi}{15}t)$, respectively. Only the relative position is assumed to be known for both adaptive control as well as PID controller. It is observed from Fig. 12 that precise landing is not possible using only PID with minimal sensors and estimation. The position errors are plotted in Fig. 13a. This shows that for a strict safe landing zone, PID controller will fail to land. Choosing a larger safe landing zone without knowing the error bounds explicitly will lead to imprecise landing or even crashes. Variation of attitude with respect to time is shown in Fig. 13b. The roll, pitch, and yaw angle variations for both cases are within $\pm 2^\circ$ which is negligible. The velocity estimate, acceleration estimate, and the tilt angles for the landing maneuver are shown in Fig. 14a, Fig. 14b, and Fig. 15, respectively.

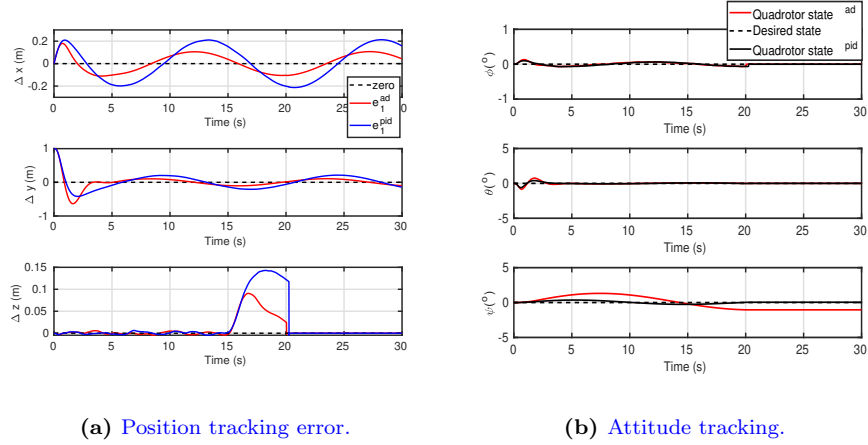


Figure 13: Position tracking error and attitude tracking for adaptive and PID controllers when landing on a moving target.

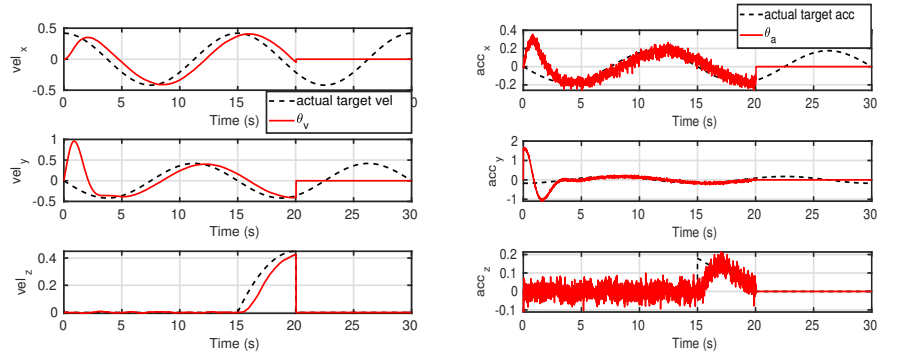


Figure 14: Simulated velocity and acceleration estimates for landing on a moving target.

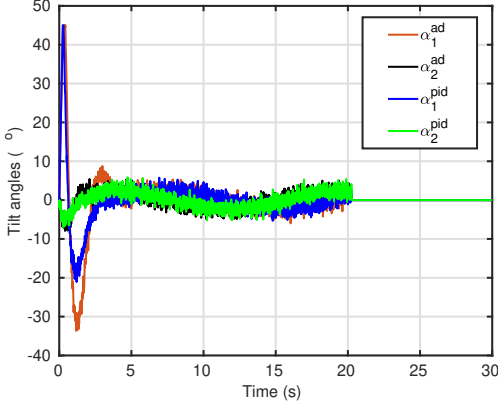


Figure 15: Tilt angles during landing on a target moving in circle simulation.

7.2. Hardware Setup

The tilt-augmented quadrotor and the ground robot used for experimental validation are described in this section. The quadrotor is completely built in-house with low-cost parts and sensors. The ground robot 0x-Delta from Nex Robotics Ltd., India [53] is used as the target for indoor experiments. A commercially available car is used for outdoor experiments.

7.2.1. Tilt-augmented Quadrotor

The vehicle used for experiments is shown in Fig. 16. It is constructed in-house at IIT Kanpur using modular components. Aluminum tubes are used for the arms and landing gear. All the electronics are mounted on multi-level balsa plates. A simple low-cost USB webcam (Genius WideCam F100) serves as the vision sensor for marker detection and is rigidly fixed to the bottom surface of the lowermost plate as shown in Fig. 17. Intel NUC (Next Unit of Computing) is used as the onboard computer/companion processor for running image-processing/vision, Kalman filter, and setpoint generator modules that are developed using ROS (Robot Operating System) Kinetic running on Ubuntu 16.04. Low-cost servo motors are used controlled by PWM signals from the autopilot. The tilting of the servo motor is limited to $\pm 45^\circ$ which is stricter

than that used for simulation experiments. Servo motor specifications can be found in [54]. The firmware for the autopilot used is the PX4 [55] open-source code base. This runs on Pixhawk autopilot hardware from 3D Robotics.

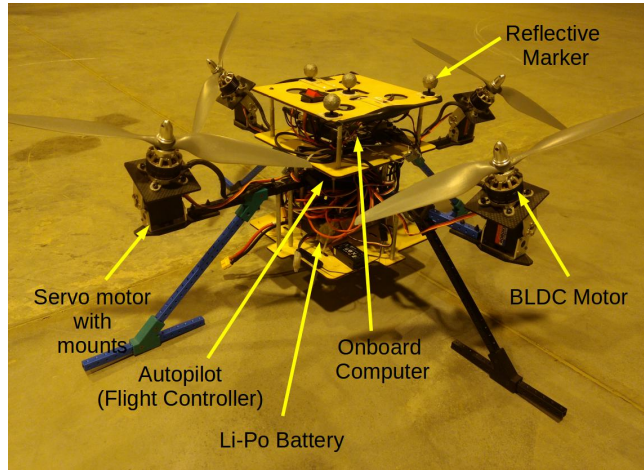


Figure 16: Vehicle prototype built and tested at Helicopter Lab, IIT Kanpur. Reflective markers are added only to record the ground truth data using a motion capture system.



Figure 17: The camera fixed on the tilt-augmented quadrotor.

The default code base uses a PID controller for attitude stabilization which is replaced by the proposed quaternion based control law given in (13). The position control module in the default firmware again uses a PID controller which is replaced by the proposed adaptive control law given in (22). The position control loop runs independently at 30 Hz and processes the estimated position of the vehicle. The control allocation is done as given in (29) and (30). A 433 MHz telemetry module is used to remotely communicate with the ground station. An Fr Sky X9D transmitter is used as the radio controller with Fr Sky X8R receiver placed onboard the vehicle and paired with the transmitter.

7.2.2. Landing Platform



Figure 18: Ground robot with the landing platform and the compound marker.

A $1 \text{ m} \times 0.8 \text{ m}$ wooden platform is added on top of the ground robot as shown in Fig. 18. Note that the dimensions of the quadrotor is approximately $0.65 \text{ m} \times 0.65 \text{ m}$. This means that the landing pad is of similar size as that of the quadrotor. This reduces the margin of error while performing the landing maneuver. On the wooden platform, the custom marker described in Section 5 is added. The ground robot is used for indoor experiments only. Hence, the platform is restricted to a maximum speed of 1 m/s. No such restrictions are

required when experiments are performed outside. The robot trajectory is manually and remotely controlled using a radio controller for all indoor experiments.

7.2.3. Modularity

One of the main objectives of this work is to build a vehicle with low-cost hardware that is fully-actuated in order to remove coupling between the position and attitude states. This reduces the complexity of tracking and landing on moving targets. This is achieved by using only IMUs on the flight controller and an onboard camera for relative pose estimation. Modularity of the hardware is highlighted by the fact that any generic quadrotor frame can be modified into a tilt-augmented quadrotor at the additional cost of only servo motors. Open source flight controllers can be modified to program any suitable control law for both position and attitude tracking. ArUco marker based detection is one of the simplest ways to extract relative pose of the target. This can be replaced by other algorithms for vision-based localization found in literature. Further, long range tracking can be enabled by using GPS. Use of GPS with the tilt-augmented quadrotor has been previously shown in [37]. Performance of the proposed methodology can be improved by using additional cost-intensive sensors and hardware like lidars and stereo cameras.

7.3. Real-world Experiments

Real-world experiments were conducted indoors using the above described tilt-augmented quadrotor and landing platform. The onboard camera streams 640×480 images at 30 Hz. The pose estimates are obtained at 20 Hz. The pose setpoints are published at 30 Hz irrespective of the marker visibility. The relative position error is set to zero when the marker goes out of frame. The image processing and the vision-based pose estimation is done on the onboard computer. This computer is also used for running the Kalman filter. The pose setpoints from the onboard computer are sent to the position and attitude controllers running on the Pixhawk using MAVLink protocol. The software setup is implemented using ROS nodes which allows asynchronous communication

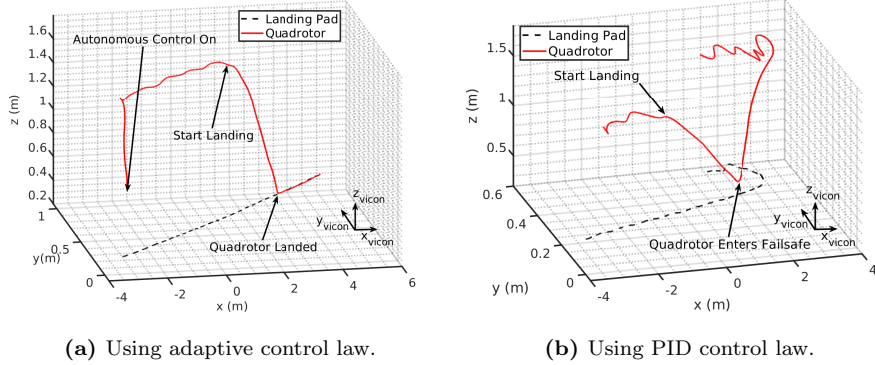


Figure 19: Ground truth for landing on a target moving in a straight line using adaptive and PID controllers.

between different parts of the program.

Three major categories of experiments are performed. Case one and two are performed indoors to collect the ground truth data using a motion capture system. Case one is where the quadrotor tracks and lands on the platform moving in a straight line. The second case is where the platform is moving in a circular trajectory similar to the simulation experiments described earlier. No communication occurs between the ground vehicle and the tilt-augmented quadrotor. The motion capture system used is Vicon Motion Capture System which provides accurate ground truth and helps validate the proposed architecture. [Comparison between adaptive and PID controllers is shown for the aforementioned indoor experiments](#). Finally, the tracking and landing on a moving car in an outdoor environment is performed. This validates the proposed methodology for targets moving at realistic speeds.

7.3.1. Landing on a Target Moving in a Straight Line

The landing platform is controlled manually to move in a straight line at a speed of approximately 0.5 m/s. The three-dimensional plot of the quadrotor and ground vehicle trajectories is given in Fig. 19 for both adaptive and PID cases. Note that the motion capture system has its own frame of reference

as indicated in Fig. 19. This is different from the inertial frame defined for the flight controller but also a non-accelerating frame. It can be seen that the adaptive control law is able to track the target faithfully and hence successfully land as shown in Fig. 19a. For the PID case, however, tracking error in the x-y plane is large and does not satisfy the precision landing bounds as set in Fig. 6. Hence, the quadrotor enters failsafe mode and ascends back to a height of 1.7 m as shown in Fig. 19b. Note that the bounds are same for both controllers.

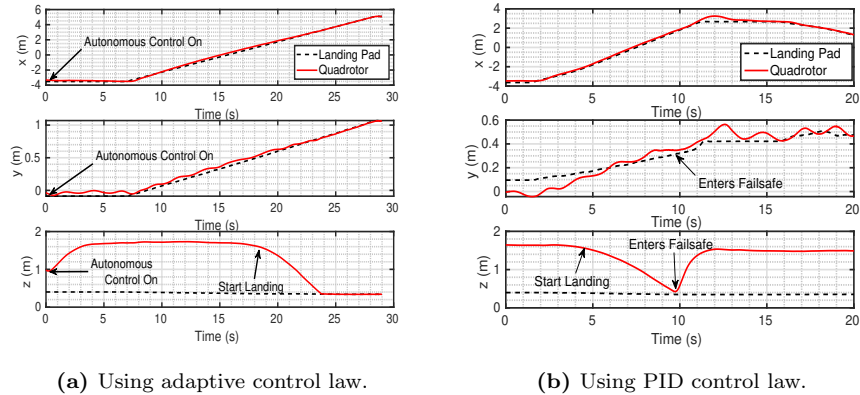


Figure 20: Position tracking and landing. Tracking in the x-y plane is better with the adaptive controller and hence precision landing is successful. The upper bound on tracking error is not satisfied by the PID controller and hence enters a failsafe mode to avoid crashing.

The position of the quadrotor and ground vehicle is plotted with respect to time in Fig. 20 for both adaptive and PID cases. The initial time, t_0 , for the landing trajectory generator is specified 15 s after switching on autonomous control. The quadrotor is commanded to follow the marker at a height of 1.7 m for that period of 15 s. The initial height is specified to be 1.7 m. Final time is decided by taking the interval $t_f - t_0 = 5$ s. The final velocity is set to 0.3 m/s. No heading information of the ground vehicle from the relative pose measurements is used in this case. The quadrotor yaw angle is free to vary in both cases but since desired yaw rate is set to zero (since $\Omega_d = 0$, as mentioned

in Section 4.1), the quadrotor tries to hold a constant heading. Slight variation in yaw is seen due to external disturbances. However, variation in yaw does not affect position tracking. Roll and pitch angles are restricted to zero and can be verified through Fig. 21. Stills from the video for the adaptive controller case are shown in Fig. 22. The corresponding stills from onboard camera are shown in Fig. 23.

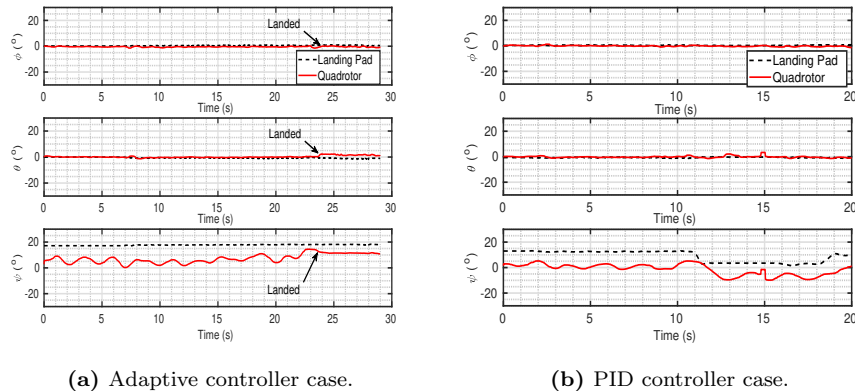


Figure 21: Attitude stabilization during landing in an indoor environment when the target is moving in a straight line. The yaw angle of landing pad is not used as setpoint in this case. However, yaw angular rate setpoint is set to zero and the quadrotor tries to hold constant yaw angle. Slight variation in yaw angle is seen due to external disturbances.

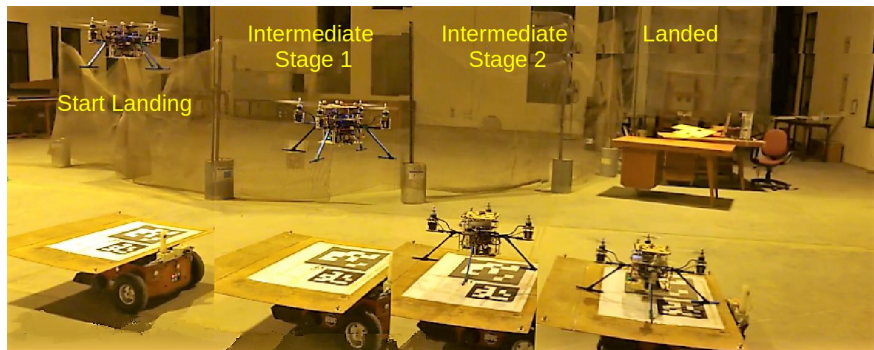


Figure 22: Stills of the indoor experiment for landing on a target moving in a straight line using the proposed adaptive control law.

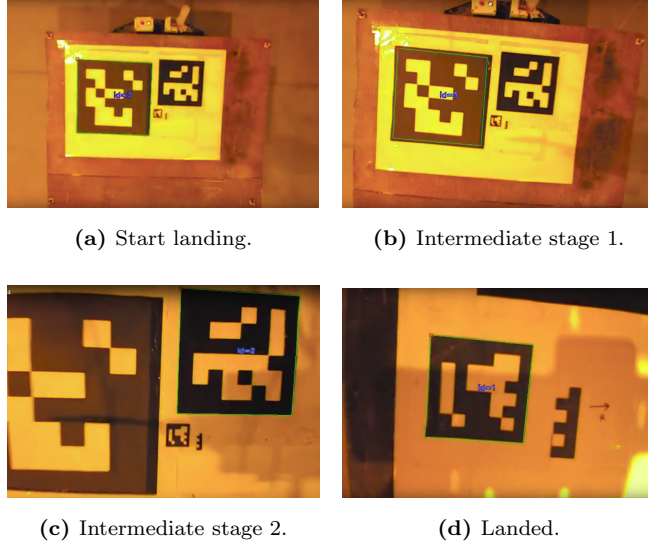
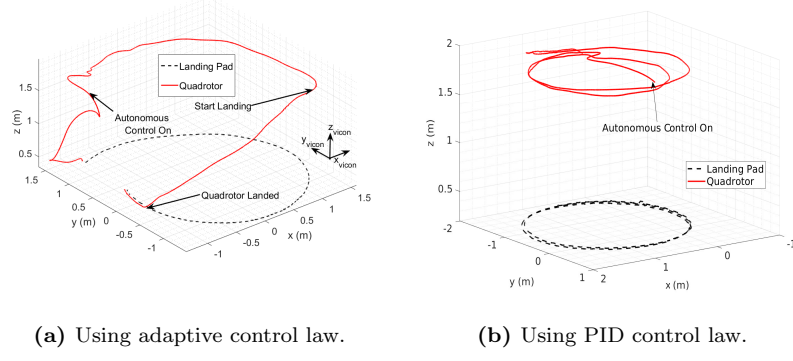


Figure 23: Video grabs from the onboard camera when landing on a target moving in a straight line using the proposed adaptive control law.

7.3.2. Landing on a Target Moving in a Circle

Landing on a ground vehicle moving in a circular trajectory is more challenging since the acceleration is continuously varying. In this section, experimental results are presented for tracking and landing on a target having a circular trajectory of radius roughly 1.2 m at an angular speed of about 0.2 rad/s. The three-dimensional plots of the quadrotor and ground vehicle trajectories for both the adaptive case as well as the PID case are given in Fig. 24. The positions of the quadrotor and ground vehicle are plotted with respect to time in Fig. 25. For the adaptive case, once the autonomous control mode is on, the quadrotor tracks the marker at a height of 1.7 m from the landing pad. The initial time, t_0 , for the landing trajectory generator is specified 20 s after switching on autonomous control. The initial height is specified to be 1.7 m. Final time is decided by taking the interval $t_f - t_0 = 10$ s. The final velocity is set to 0.3 m/s. For the PID case, tracking the target at a constant height of 1.7 m is shown. The quadrotor is unable to follow the target without introducing large

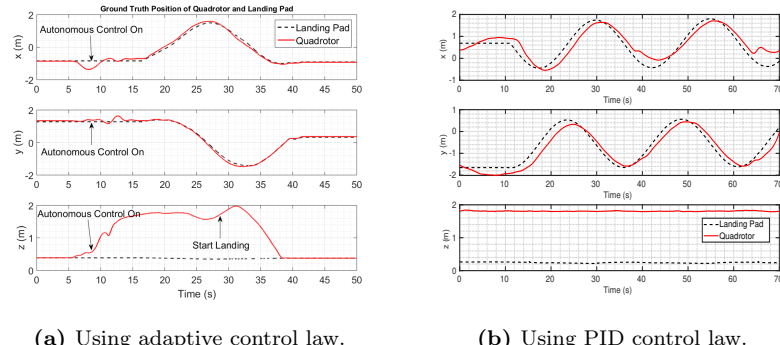
errors in the x-y plane. Hence, landing is not attempted using PID. Attitude tracking for both cases is shown in Fig. 26. The heading information of the ground vehicle is used in this case from the relative pose measurements from the ArUco marker detection node. Stills from the video during landing using the proposed adaptive control law are shown in Fig. 27. The corresponding stills from onboard camera are shown in Fig. 28.



(a) Using adaptive control law.

(b) Using PID control law.

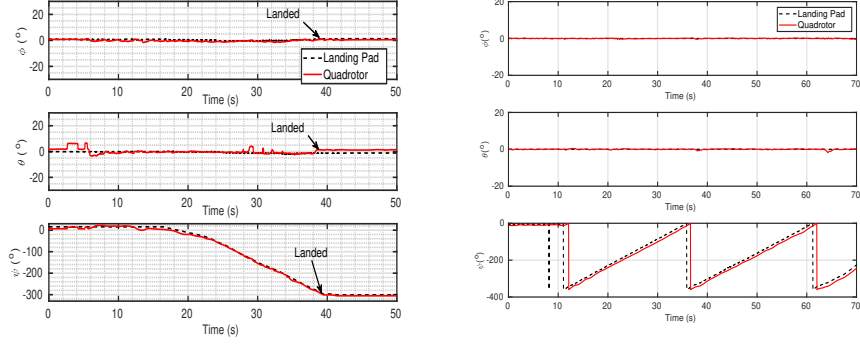
Figure 24: Ground truth for (a) landing on a target moving in a circle using adaptive control law. (b) tracking a target moving in a circle using the PID controller. Landing is not attempted with PID as tracking performance is poor without velocity estimate.



(a) Using adaptive control law.

(b) Using PID control law.

Figure 25: Position tracking using the proposed adaptive control law and PID. The quadrotor is able to track and successfully land on the target while using the proposed adaptive control law. Since tracking performance is poor without velocity estimate in the case of PID controller, landing is not attempted.



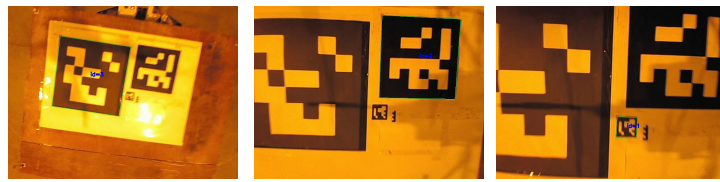
(a) Adaptive controller case.

(b) PID controller case.

Figure 26: Attitude stabilization during landing in an indoor environment when the target is moving in a circle. The quadrotor is commanded to follow the marker's yaw angle in both cases. Since the attitude controller is unchanged, the attitude tracking response is similar.



Figure 27: Stills from the video for landing on a target moving in a circle when using the proposed adaptive control law.



(a) Start landing.

(b) Intermediate stage.

(c) About to land.

Figure 28: Stills from the onboard camera for landing on a target moving in a circle when using the proposed adaptive control law.

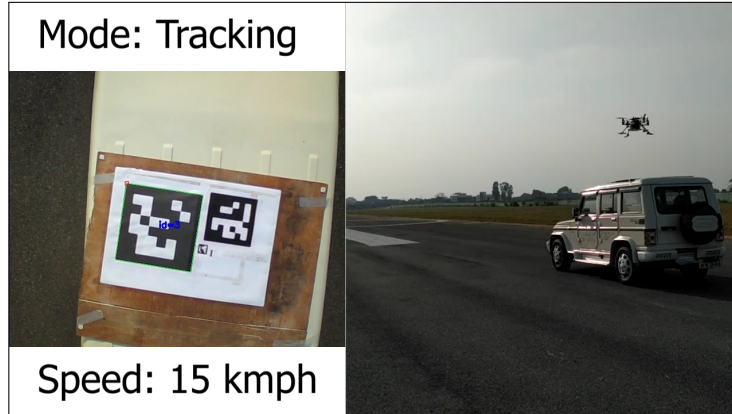


Figure 29: Tracking a car moving at a speed of 15 km/h.

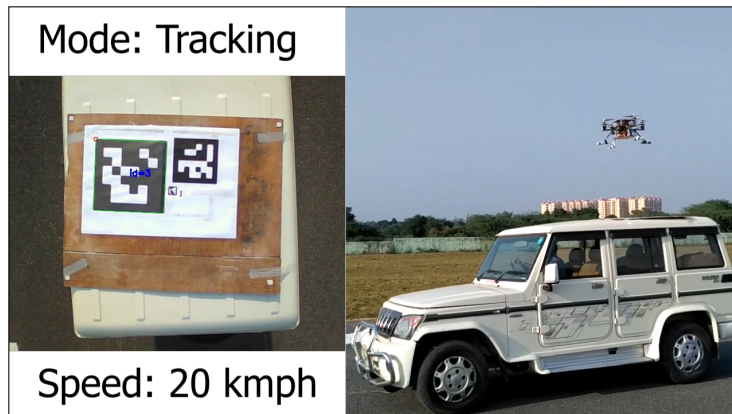


Figure 30: Tracking a car moving at a speed of 20 km/h.

7.3.3. Tracking and Landing on a Moving Car

To demonstrate the real-world applicability of the proposed architecture, tracking a moving car in an outdoor environment is performed along with successful landing at higher speeds. The experiments are carried out with the car moving at 15 km/h and 20 km/h. The tilt-augmented quadrotor tracks the car with negligible changes in attitude. Tracking is performed for a duration of 20 s, after which the landing generator provides the trajectory along the z_i -axis. The difference between initial and final time for the landing trajectory generator is

given to be $t_f - t_0 = 10$ s. Stills from the videos of the experiments are shown in Fig. 29 and Fig. 30. The experiments show the feasibility of the approach to real-life scenarios. Note that the maximum velocity that can be tracked is only limited by the maximum horizontal velocity of the tilt-augmented quadrotor. The maximum horizontal speed of the tilt-augmented quadrotor is shown to be comparable to that of a normal quadrotor in [37].

8. Discussion and Summary

This paper discussed in detail the autonomous tracking and landing of a tilt-augmented quadrotor on a moving target. A tilt-augmented quadrotor is fully-actuated, unlike a conventional rotorcraft. The additional degrees of freedom allow the UAV to be controlled in such a way that the position and attitude states are decoupled. The mathematical modeling of the novel, fully-actuated quadrotor was discussed. The expressions for the control inputs of the tilt-augmented quadrotor were derived which revealed the necessity for careful control allocation.

One of the main aims of this work was to use low-cost hardware to achieve vision-based tracking and landing. To this end, a minimum sensor suite was used consisting of IMUs and low-cost onboard camera. This implied that only relative pose measurements were available without any information about the target velocity or acceleration. Traditional PID controllers fail to achieve satisfactory tracking without the target's velocity or acceleration information. This was demonstrated through numerical simulations. To improve tracking performance, an adaptive control law was proposed that estimated the target velocity and acceleration. It was shown through Lyapunov stability theory that the position and velocity errors asymptotically converge to zero when the target moves at a constant velocity. It was also shown that the errors remain bounded when the target acceleration was non-zero but finite. A simple attitude control law using quaternions was given to stabilize the roll and pitch to zero while tracking yaw angle commands. Vision-based localization was done using ArUco markers

and simple open-source algorithms for target pose estimation. This was implemented using ROS which allows the system to be expanded to any possible pose estimation algorithm. Compound markers were used to achieve precise localization which in turn improved the precision of tracking and landing. Minimum acceleration trajectories for landing were generated to overcome disturbances due to ground effect during landing. A conical safe landing zone was defined for a given camera field of view and for a given error tolerance for landing. This prevents the quadrotor from attempting landing if the tracking is poor.

The proposed architecture was validated using both numerical simulations as well as real-world experiments. A comparison between the proposed adaptive control law and PID controllers showed that the adaptive control law has superior tracking capabilities when the information available is minimal. Real-world experiments were performed both indoors and outdoors to show the effectiveness of the proposed methodology. As expected, the tilt-augmented quadrotor was able to track and land on moving targets with the help of only low-cost onboard sensors.

Acknowledgments

This work is supported by Science and Engineering Research Board, Government of India (project number SERB/EE/2018172). The authors thank the Flight Lab and the Helicopter Lab at IIT Kanpur for their support while conducting the experiments.

References

- [1] J. P. How, C. Fraser, K. C. Kulling, L. F. Bertuccelli, O. Toupet, L. Brunet, A. Bachrach, N. Roy, Increasing autonomy of uavs, *IEEE Robotics & Automation Magazine* 16 (2) (2009) 43–51.
- [2] B. Kim, M. Kaess, L. Fletcher, J. Leonard, A. Bachrach, N. Roy, S. Teller, Multiple relative pose graphs for robust cooperative mapping, in: *IEEE*

- International Conference on Robotics and Automation (ICRA), 2010, pp. 3185–3192.
- [3] N. Michael, S. Shen, K. Mohta, V. Kumar, K. Nagatani, Y. Okada, S. Kiribayashi, K. Otake, K. Yoshida, K. Ohno, et al., Collaborative mapping of an earthquake damaged building via ground and aerial robots, in: Field and Service Robotics, Springer, 2014, pp. 33–47.
 - [4] I. F. Mondragón, P. Campoy, C. Martinez, M. A. Olivares-Méndez, 3d pose estimation based on planar object tracking for uavs control, in: 2010 IEEE international conference on Robotics and automation (ICRA), 2010, pp. 35–41.
 - [5] C. Teuliere, L. Eck, E. Marchand, Chasing a moving target from a flying uav, in: Intelligent Robots and Systems (IROS), 2011 IEEE/RSJ International Conference on, IEEE, 2011, pp. 4929–4934.
 - [6] S. Huh, D. H. Shim, A vision-based landing system for small unmanned aerial vehicles using an airbag, Control Engineering Practice 18 (7) (2010) 812–823.
 - [7] J. Courbon, Y. Mezouar, N. Guénard, P. Martinet, Vision-based navigation of unmanned aerial vehicles, Control Engineering Practice 18 (7) (2010) 789–799.
 - [8] S. A. Quintero, J. P. Hespanha, Vision-based target tracking with a small uav: Optimization-based control strategies, Control Engineering Practice 32 (2014) 28–42.
 - [9] J. Thomas, J. Welde, G. Loianno, K. Daniilidis, V. Kumar, Autonomous flight for detection, localization, and tracking of moving targets with a small quadrotor, IEEE Robotics and Automation Letters 2 (3) (2017) 1762–1769.
 - [10] J. Kim, Y. Jung, D. Lee, D. H. Shim, Outdoor autonomous landing on a moving platform for quadrotors using an omnidirectional camera, in:

International Conference on Unmanned Aircraft Systems (ICUAS), IEEE, 2014, pp. 1243–1252.

- [11] D. Lee, T. Ryan, H. J. Kim, Autonomous landing of a vtol uav on a moving platform using image-based visual servoing, in: IEEE International Conference on Robotics and Automation (ICRA), IEEE, 2012, pp. 971–976.
- [12] K. Ling, Precision landing of a quadrotor uav on a moving target using low-cost sensors, Master’s thesis, University of Waterloo (2014).
- [13] S. Saripalli, J. F. Montgomery, G. S. Sukhatme, Visually guided landing of an unmanned aerial vehicle, *IEEE Transactions on Robotics and Automation* 19 (3) (2003) 371–380.
- [14] S. Saripalli, G. S. Sukhatme, Landing on a moving target using an autonomous helicopter, in: Field and Service Robotics, Springer, 2003, pp. 277–286.
- [15] T. S. Richardson, C. G. Jones, A. Likhoded, E. Sparks, A. Jordan, I. Cowling, S. Willcox, Automated vision-based recovery of a rotary wing unmanned aerial vehicle onto a moving platform, *Journal of Field Robotics* 30 (5) (2013) 667–684.
- [16] L. Wang, X. Bai, Quadrotor autonomous approaching and landing on a vessel deck, *Journal of Intelligent & Robotic Systems* 92 (1) (2018) 125–143.
- [17] O. Araar, N. Aouf, I. Vitanov, Vision based autonomous landing of multirotor uav on moving platform, *Journal of Intelligent & Robotic Systems* 85 (2) (2017) 369–384.
- [18] B. Hu, L. Lu, S. Mishra, A control architecture for time-optimal landing of a quadrotor onto a moving platform, *Asian Journal of Control* 20 (5) (2018) 1701–1712.

- [19] A. Rodriguez-Ramos, C. Sampedro, H. Bavle, Z. Milosevic, A. Garcia-Vaquero, P. Campoy, Towards fully autonomous landing on moving platforms for rotary unmanned aerial vehicles, in: International Conference on Unmanned Aircraft Systems (ICUAS), IEEE, 2017, pp. 170–178.
- [20] P. Serra, R. Cunha, T. Hamel, D. Cabecinhas, C. Silvestre, Landing of a quadrotor on a moving target using dynamic image-based visual servo control, *IEEE Transactions on Robotics* 32 (6) (2016) 1524–1535.
- [21] P. Vlantis, P. Marantos, C. P. Bechlioulis, K. J. Kyriakopoulos, Quadrotor landing on an inclined platform of a moving ground vehicle, in: IEEE International Conference on Robotics and Automation (ICRA), IEEE, 2015, pp. 2202–2207.
- [22] A. Gautam, P. Sujit, S. Saripalli, A survey of autonomous landing techniques for uavs, in: Unmanned Aircraft Systems (ICUAS), 2014 International Conference on, IEEE, 2014, pp. 1210–1218.
- [23] S. Jin, J. Zhang, L. Shen, T. Li, On-board vision autonomous landing techniques for quadrotor: A survey, in: 35th Chinese Control Conference (CCC), IEEE, 2016, pp. 10284–10289.
- [24] D. Falanga, A. Zanchettin, A. Simovic, J. Delmerico, D. Scaramuzza, Vision-based autonomous quadrotor landing on a moving platform, in: Proceedings of the IEEE International Symposium on Safety, Security and Rescue Robotics, Shanghai, China, 2017, pp. 11–13.
- [25] A. Borowczyk, D.-T. Nguyen, A. Phu-Van Nguyen, D. Q. Nguyen, D. Saussié, J. Le Ny, Autonomous landing of a multirotor micro air vehicle on a high velocity ground vehicle, *IFAC-PapersOnLine* 50 (1) (2017) 10488–10494.
- [26] T. Baca, P. Stepan, M. Saska, Autonomous landing on a moving car with unmanned aerial vehicle, in: Mobile Robots (ECMR), 2017 European Conference on, IEEE, 2017, pp. 1–6.

- [27] F. Bullo, A. D. Lewis, Geometric control of mechanical systems: modeling, analysis, and design for simple mechanical control systems, Vol. 49, Springer Science & Business Media, 2004.
- [28] P. Marantos, G. C. Karras, P. Vlantis, K. J. Kyriakopoulos, Vision-based autonomous landing control for unmanned helicopters, *Journal of Intelligent & Robotic Systems* (2017) 1–14.
- [29] M. Gašparović, L. Jurjević, Gimbal influence on the stability of exterior orientation parameters of uav acquired images, *Sensors* 17 (2) (2017) 401.
- [30] S. Tobin Fisher, J. B. Van Niekerk, C. Janik, Miniature stabilized unmanned aerial vehicle gimbal, uS Patent App. 15/087,996 (Mar. 2016).
- [31] M. Ryll, H. H. Bülthoff, P. R. Giordano, Modeling and control of a quadrotor uav with tilting propellers, in: *IEEE International Conference on Robotics and Automation (ICRA)*, IEEE, 2012, pp. 4606–4613.
- [32] M. Ryll, H. H. Bülthoff, P. R. Giordano, A novel overactuated quadrotor unmanned aerial vehicle: Modeling, control, and experimental validation, *IEEE Transactions on Control Systems Technology* 23 (2) (2015) 540–556.
- [33] F. Şenkul, E. Altug, Modeling and control of a novel tiltroll rotor quadrotor uav, in: *International Conference on Unmanned Aircraft Systems (ICUAS)*, IEEE, 2013, pp. 1071–1076.
- [34] A. Nemati, M. Kumar, Modeling and control of a single axis tilting quadcopter, in: *American Control Conference (ACC)*, 2014, IEEE, 2014, pp. 3077–3082.
- [35] A. Oosedo, S. Abiko, S. Narasaki, A. Kuno, A. Konno, M. Uchiyama, Flight control systems of a quad tilt rotor unmanned aerial vehicle for a large attitude change, in: *IEEE International Conference on Robotics and Automation (ICRA)*, IEEE, 2015, pp. 2326–2331.

- [36] R. Kumar, A. Nemati, M. Kumar, R. Sharma, K. Cohen, F. Cazaurang, Tilting-rotor quadcopter for aggressive flight maneuvers using differential flatness based flight controller, in: ASME 2017 Dynamic Systems and Control Conference, American Society of Mechanical Engineers, 2017.
- [37] M. Bhargavapuri, J. Patrikar, S. R. Sahoo, M. Kothari, A low-cost tilt-augmented quadrotor helicopter : Modeling and control, in: 2018 International Conference on Unmanned Aircraft Systems (ICUAS), 2018, pp. 186–194.
- [38] F. J. Romero-Ramirez, R. Muoz-Salinas, R. Medina-Carnicer, Speeded up detection of squared fiducial markers, *Image and Vision Computing* 76 (2018) 38 – 47.
- [39] N. Gupta, M. Kothari, Abhishek, Flight dynamics and nonlinear control design for variable-pitch quadrotors, in: 2016 American Control Conference (ACC), 2016, pp. 3150–3155.
- [40] R. Mahony, V. Kumar, P. Corke, Multirotor aerial vehicles: Modeling, estimation, and control of quadrotor, *IEEE Robotics and Automation magazine* 19 (3) (2012) 20–32.
- [41] M. Cutler, J. P. How, Actuator constrained trajectory generation and control for variable-pitch quadrotors, in: AIAA Guidance, Navigation, and Control Conference (GNC), 2012.
- [42] E. Fresk, G. Nikolakopoulos, Full quaternion based attitude control for a quadrotor, in: European Control Conference (ECC), IEEE, 2013, pp. 3864–3869.
- [43] M. Bhargavapuri, S. R. Sahoo, M. Kothari, Global attitude stabilization using pseudo-targets, 2018, arXiv preprint, arXiv:1811.01924.
- [44] H. Lee, H. J. Kim, Trajectory tracking control of multirotors from modelling to experiments: A survey, *International Journal of Control, Automation and Systems* 15 (1) (2017) 281–292.

- [45] H. Mo, G. Farid, Nonlinear and adaptive intelligent control techniques for quadrotor uav—a survey, *Asian Journal of Control*, 2019.
- [46] F. Kendoul, Survey of advances in guidance, navigation, and control of unmanned rotorcraft systems, *Journal of Field Robotics* 29 (2) (2012) 315–378.
- [47] Y. Li, S. Song, A survey of control algorithms for quadrotor unmanned helicopter, in: 2012 IEEE Fifth International Conference on Advanced Computational Intelligence (ICACI), 2012, pp. 365–369.
- [48] M. Kamel, S. Verling, O. Elkhattib, C. Sprecher, P. Wulkop, Z. Taylor, R. Siegwart, I. Gilitschenski, Voliro: An omnidirectional hexacopter with tilttable rotors, arXiv preprint arXiv:1801.04581.
- [49] S. Garrido-Jurado, R. Muñoz-Salinas, F. J. Madrid-Cuevas, M. J. Marín-Jiménez, Automatic generation and detection of highly reliable fiducial markers under occlusion, *Pattern Recognition* 47 (6) (2014) 2280–2292.
- [50] G. Bradski, The OpenCV Library, *Dr. Dobb's Journal of Software Tools*.
- [51] G. Bishop, G. Welch, et al., An introduction to the kalman filter, Proc of SIGGRAPH, Course 8 (27599-3175) (2001) 59.
- [52] D. Mellinger, V. Kumar, Minimum snap trajectory generation and control for quadrotors, in: 2011 IEEE International Conference on Robotics and Automation (ICRA), IEEE, 2011, pp. 2520–2525.
- [53] N. R. P. Ltd., 0x-delta 4 wheel drive robot, online (2017).
URL <http://www.nex-robotics.com/products/0x-series-robots/0x-delta-4-wheel-drive-robot.html>
- [54] I. Robokits, Metal gear dual shaft 16kgcm digital servo motorOnline.
URL <https://robokits.co.in/motors/rc-servo-motors/metal-gear-dual-shaft-16kgcm-digital-servo-motor>

- [55] L. Meier, D. Honegger, M. Pollefeys, Px4: A node-based multithreaded open source robotics framework for deeply embedded platforms, in: IEEE International Conference on Robotics and Automation (ICRA), 2015, IEEE, 2015, pp. 6235–6240.